GEOLOGICAL JOURNAL
Geol. J. **41**: 123–143 (2006)
Published online in Wiley InterScience (www.interscience.wiley.com). DOI: 10.1002/gj.1037

Intrusive lherzolites within the basalts of Küre ophiolite (Turkey): an occurrence in the Tethyan suprasubduction marginal basin

ÜNER ÇAKIR[1], YURDAL GENÇ[1] and DOĞAN PAKTUNÇ[2]*

[1]*Hacettepe Üniversitesi, Mühendislik Fakültesi, Jeoloji Mühendisliği Bölümü, Beytepe, TR-06532 Ankara, Turkey*

[2]*Canada Centre for Mineral and Energy Technology, 555 Booth Street, Ottawa, Canada*

The Küre ophiolite is interpreted as the remnants of the suprasubduction marginal basin formed on the northwardly subducted Tethyan oceanic lithosphere. The Küre Basin was opened during late Late Triassic and closed during late Middle Jurassic.

Intrusive lherzolites cut the lower part of the basalts forming the volcanic upper unit of the Küre ophiolite. Lherzolites occur in tabular form with hectometric dimensions and have a massive character. High temperature metamorphic effects were developed in the wallrock along a zone a few metres thick. The lherzolite is relatively fresh and displays poikilitic texture where subhedral and anhedral olivines are included in large pyroxenes. The primary mineral paragenesis of the lherzolite is represented by olivine and chromite as early cumulus phases. Diopside, bronzite and plagioclase are the late igneous minerals. Hornblende and titanite formed during the late stage of crystallization at the expense of clinopyroxene. Serpentine minerals, phlogopite and hydrogrossular are the secondary minerals formed at the expense of olivine, bronzite and diopside. Tremolite, actinolite, chlorite and sericite are the late alteration products of the lherzolite.

High temperature and low pressure conditions are indicated based on the mineral compositions. The crystallization temperature of the olivine and chromite is estimated to be 1015–1070°C, and that of the pyroxenes, the last crystallized primary minerals, around 900–950°C. The solidification of the magma was completed in the lower part of the basalts, at a depth of *c.* 2.7 km. The Küre lherzolite has a very high oxygen fugacity indicating an oxidized arc magma origin. The magma rose as a crystal mush and intruded the basalts. The generation of the parental magma may be explained by extensive melting of the upper mantle, facilitated by the presence of hydrous fluids released from the subducted Tethyan oceanic lithosphere.

Received 23 November 2003; revised version received 2 January 2006; accepted 20 January 2006

KEY WORDS Küre ophiolite; intrusive lherzolite; P–T estimates; marginal basin, Turkey

1. INTRODUCTION

Intrusive lherzolites within the oceanic crustal sequence are of interest to geologists because of their rarity in ophiolites, possibly due to the difficulty of emplacing dense peridotitic magma in the crust. The Küre ophiolite is one of the rare massifs displaying late intrusive peridotites and is unique due to the presence of lherzolitic bodies cutting the basalts.

The Küre ophiolite is a small oceanic assemblage which is principally known for its Cyprus-type massive sulphide deposits (Mitchell and Bell 1973; Erler 1995). A renewed interest developed when it was considered as a 'fragment of the Permian–Triassic Palaeotethyan oceanic lithosphere' (Şengör *et al.* 1980). Until that time

* Correspondence to: Ü. Çakir, Hacettepe Üniversitesi, Mühendislik Fakültesi, Jeoloji Mühendisliği Bölümü, Beytepe, TR-06532 Ankara, Turkey.
E-mail: ucakir@hacettepe.edu.tr

it was generally accepted that, from Late Carboniferous to Early Triassic, oceanic lithosphere was not present between Laurasia and Gondwanaland in the Anatolian region (Argyriadis 1975).

Palaeontological and geochronological data (Aydin *et al.* 1995; Kozur *et al.* 2000; Terzioğlu *et al.* 2000) indicate that the Küre Basin was open between Late Triassic and late Middle Jurassic. Geochemical trace element data of the basalts suggest that the Küre ophiolite represents the fragments of a marginal basin generated above a subduction zone (Ustaömer and Robertson 1993, 1994, 1995, 1997, 1999; Boztuğ *et al.* 1995; Kozur *et al.* 2000) rather than a piece of the major oceanic lithosphere. As a consequence, the Küre lherzolite may be interpreted as being formed, in Jurassic time, in a marginal basin above the subducted oceanic lithosphere. A similar setting was proposed for the intrusive peridotites cross-cutting the pyroxenitic and gabbroic cumulates of the Troodos ophiolite (Laurent 1992).

This paper is based on the results of a detailed field-based geological study on the Küre ophiolite. It aims to describe geological, petrographical and geochemical characterististics of the Küre lherzolites and to discuss the question of whether there is a link between the emplacement of the lherzolite and the geodynamical environment.

2. GEOLOGY OF THE KÜRE OPHIOLITE

The Küre ophiolite is a small oceanic assemblage situated in the Central Pontides, about 20 km to the south of the Black Sea coast (Figure 1). It consists of harzburgite to dunitic tectonites, basaltic volcanics and detrital sedimentary units, intrusive lherzolites and gabbros (Figure 2). The harzburgites, dunites, basalts and shale–sandstone units are cut by isolated diabase dykes. Ustaömer and Robertson (1993, 1994) report also a true sheeted dyke complex cutting the isotropic microgabbros. All units are intruded by Middle Dogger granitoids (Boztuğ *et al.* 1995) and are covered unconformably by conglomerates of late Dogger–early Malm age followed by Malm limestones (Güner 1980; Pehlivanoğlu 1985; Aydin *et al.* 1986; Ustaömer and Robertson 1994; Çakır 1995).

The contacts between different ophiolitic units are generally tectonic within an imbricated structure (Figure 1). The harzburgites and dunites occur as tectonic slices on top of the volcanic and detrital sedimentary rocks. The basalts are often overthrust onto the shale–sandstone unit. However, in the Aşıköy mine area, west of Küre town, the primary relationship of basalts at the bottom, and orebody and shale–sandstone at the top, is well observed (Figure 2). These units have a normal contact relationship and they constitute a ridge (Aşıköy ridge) with a general trend of N38°W. They are generally offset by normal faults which tend to be parallel to the ridge axis. It is important to point out that various geological elements observed in the volcanic and sedimentary units are parallel to each other and oriented in a NW–SE direction. In particular, the parallel orientation of diabase dykes, lherzolites and gabbro intrusions to the Aşıköy ridge axis points to an early spreading ridge structure formed in the oceanic environment. Consequently, the parallelism of normal faults and ridge axis and formation of a horst-graben system becomes explainable. Bailey *et al.* (1967) suggest that these faults were formed before the formation of the massive sulphide deposits and created the channels for the mineralizing solutions.

The basalts are represented by massive basaltic lavas, pillow lavas and hyaloclastites. They form the host and footwall rocks of the Küre massive sulphide deposits. In the Aşıköy area they are covered conformably by a shale–sandstone unit. Evidence from the Aşıköy open pit and underground mine area together with drill cores document that at the upper levels the sequence contains basalt–shale alternations (Çakır 1995). The major and trace element analyses and pyroxene chemistry of the basalts are consistent with mid-ocean ridge basalt (MORB) and voloanic arc basalt (VAB) compositions (Ustaömer and Robertson 1994, 1999). The available whole-rock ages from the basalts are 170 ± 6 Ma (Aydin *et al.* 1995) and 168 ± 5 Ma (Terzioğlu *et al.* 2000). Although the whole-rock ages should be treated with caution due to the probable extensive low-temperature alteration effects, they are supported by palaeontological data of Önder *et al.* (1987).

The shale–sandstone unit constitutes the main part of the Küre ophiolite. Around Çal village, 20 km SE of Küre town (Figure 1), dark-grey marly siltstones and shales of Rhaetian age overlie the Upper Triassic passive marginal limestones comparable with the North Alpine-type Halstatt Limestones (Kozur *et al.* 2000). Around the Göynükdağı region, shale–sandstone alternations conformably overlie biomicritic limestones of the Kayabaşı Formation

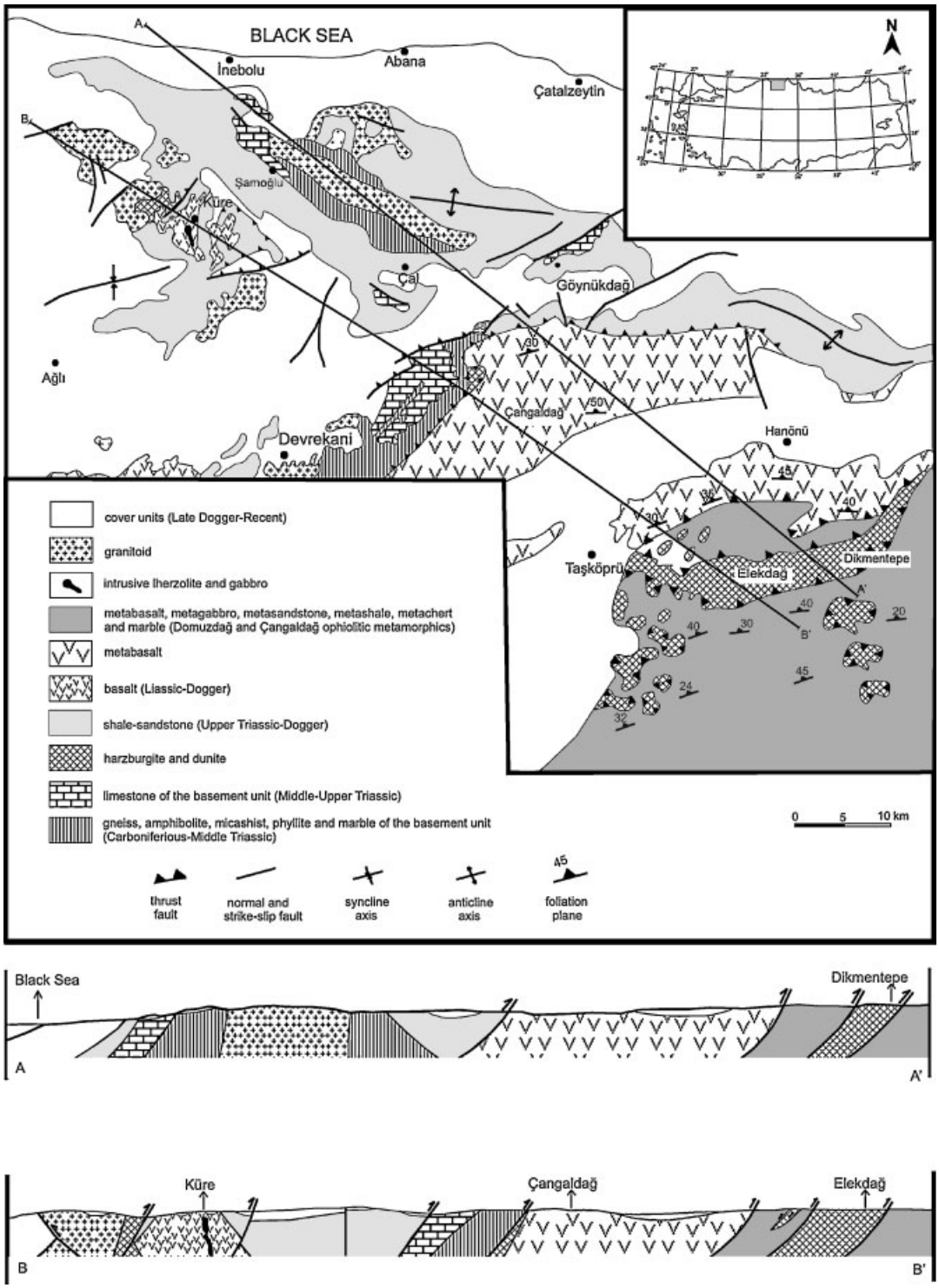

Figure 1. General geological map and cross-sections of Küre–Cangaldağ–Elekdağ ophiolites. Compiled and modified from Eren (1979), Yılmaz (1980), Aydın *et al.* (1986) and Çakır (1995).

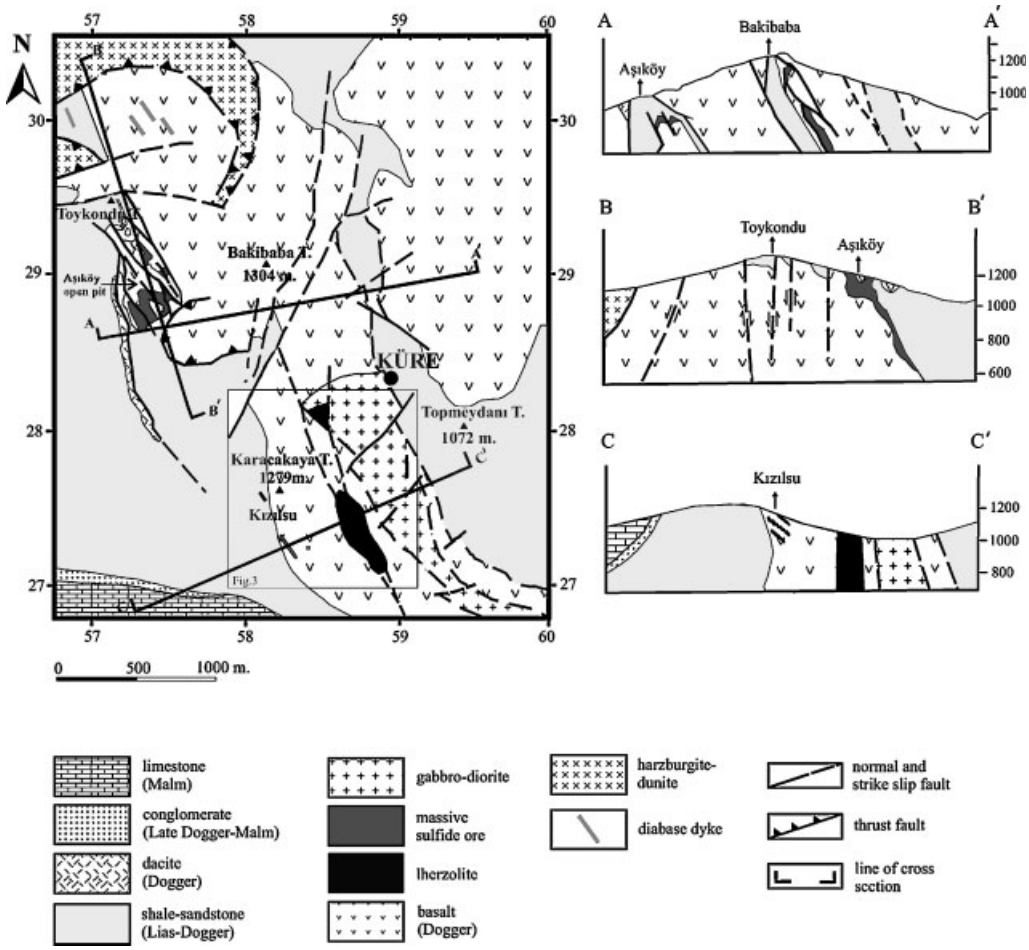

Figure 2. Geological map and cross-sections of Küre area. Modified from Güner (1980), Pehlivanoğlu (1985), JICA and MMAJ (1992) and Çakır (1995).

dated to be Middle–Late Triassic by macro- and microfossils (Önder *et al.* 1987). Around Şamoğlu village, 12 km NE of Küre town, shale–sandstone alternations overlie shallow-water limestones of Early and Middle Triassic age (Sırçalık Formation) and metamorphic rocks with an angular unconformity (Pehlivanoğlu 1985; Aydin *et al.* 1995).

The metamorphic rocks, representing the continental basement of the Central Pontides, are composed, from bottom to top, of gneisses, micaschists, amphibolites, marbles and phyllites. The K-Ar age of the lowermost gneiss is 311 ± 6.2 Ma (Aydin *et al.* 1995).

The geological setting of the shale–sandstone unit (the Akgöl Formation; Ketin and Gümüş 1962), covering both the oceanic and surrounding continental units in a small area, shows that the Küre ophiolite was formed in a narrow marginal basin which opened during late Late Triassic time. The Akgöl Formation contains few fossils indicative of Late Triassic–Liassic (Aydin *et al.* 1986, 1995), Liassic (Kovenko 1944; Ketin 1962) and Dogger (Önder *et al.* 1987) ages. Some Upper Carboniferous and Lower Permian palynomorphs reported from the formation (Kutluk and Bozdoğan 1981) are interpreted as reworked material from the older adjacent units (Yilmaz and Şengör 1985; Ustaömer and Robertson 1994; Kozur *et al.* 2000).

The Küre ophiolite is covered unconformably by basal conglomerates of late Dogger–early Malm age (Aydin *et al.* 1995). Accordingly, it appears that the oceanic life of the Küre ophiolite was constrained between Liassic and late Dogger.

3. GEOLOGICAL SETTING OF THE KÜRE LHERZOLITE

Lherzolites occur south of Küre town as two outcrops and probably represent different parts of the same intrusive body (Figure 3). The first lherzolite outcrop is located east of the hill of Karacakaya and has a lenticular body with a thickness of 75–100 m and length of 400 m. The strike is N37°W with a dip of 70–80° to the SW. In general, the contacts between lherzolite and basalt are faulted. Nevertheless, sometimes the primary nature of the contact can be observed with magmatic zoning in the lherzolite and high-temperature metamorphic effects in the basalt. The relationships suggest that lherzolite was emplaced into the fractures opened during the oceanic period. Lherzolite is massive with a greenish black colour (Figure 4a). It is relatively fresh and displays poikilitic texture where subhedral and anhedral olivines are included in large pyroxenes (Figure 4b). Near the contacts with the basalts, the lherzolite displays brecciation. This brecciation appears to have occurred during the final stages of the emplacement and crystallization of the ultrabasic magma as the host basaltic rocks do not display brecciation. At the contact zone lherzolite progressively grades into plagioclase lherzolite and olivine gabbro lithologies. This zone is normally 2–5 m thick, and composed of olivine, plagioclase, bronzite, diopside, chromium spinel and magnetite.

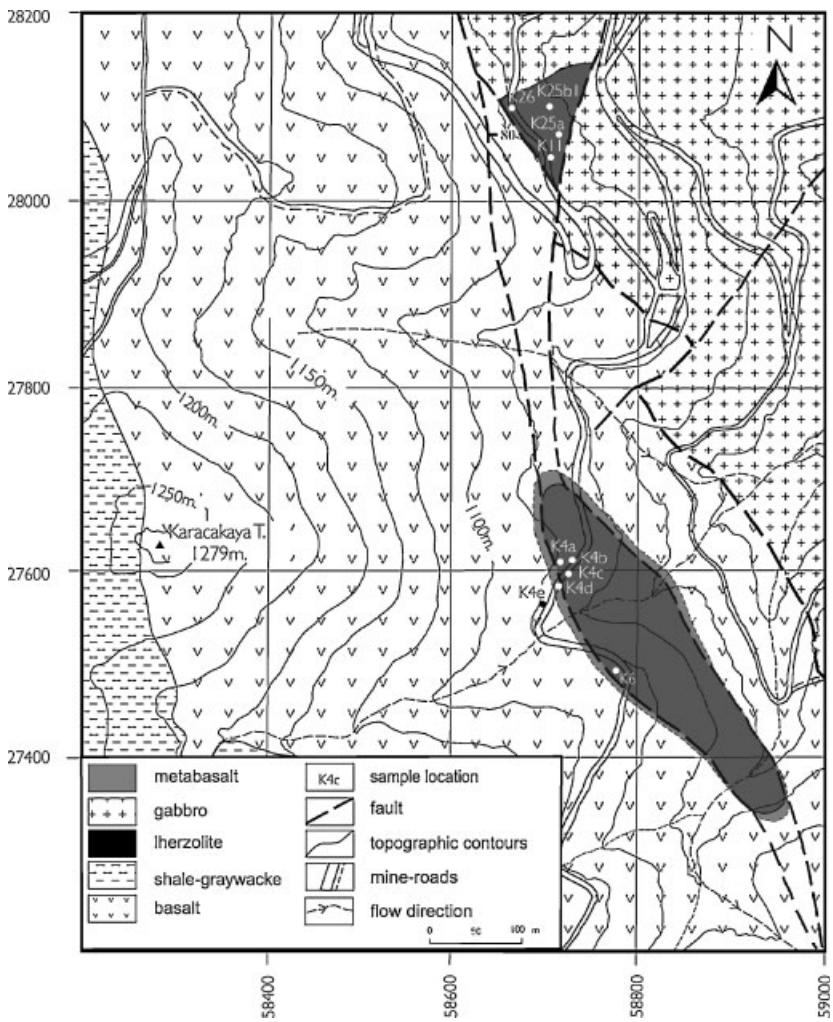

Figure 3. Detailed geological map of the lherzolite intrusions.

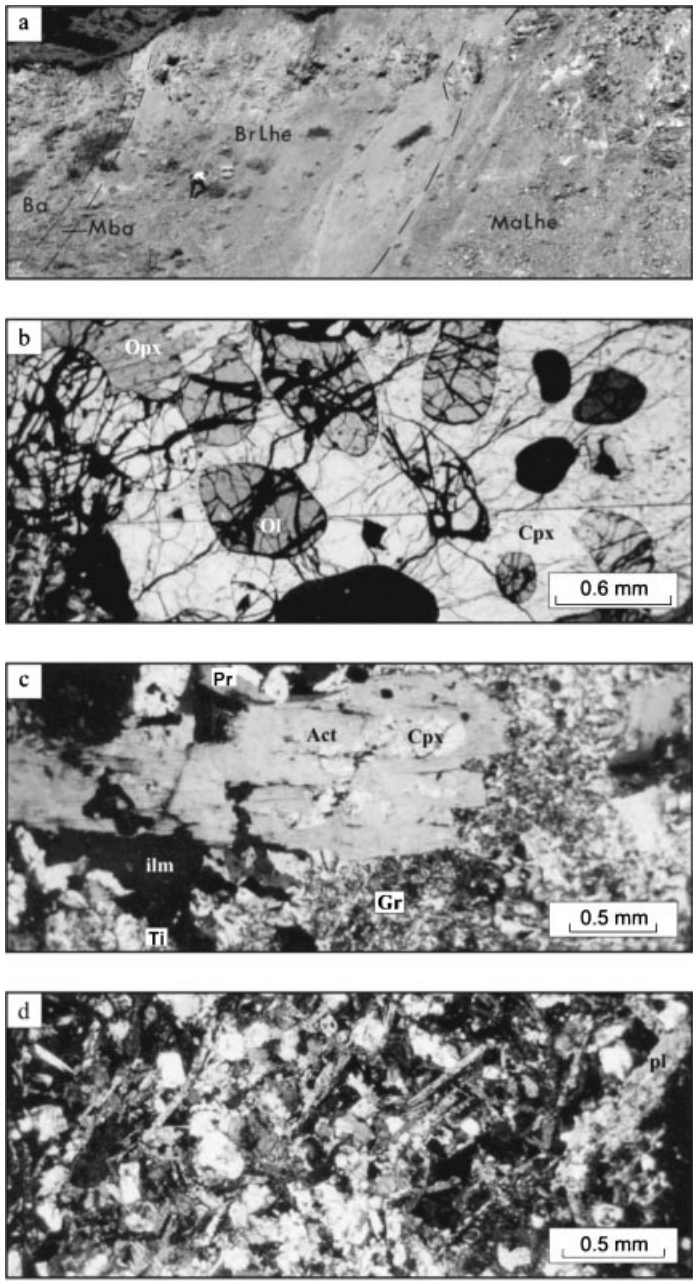

Figure 4. Field and microcopic views of the intrusive lherzolites and the wall rocks. (**a**) General view of the intrusive lherzolite east of Karacakaya tepe. Ba, basalt; BrLhe, brecciated lherzolite; MaLhe, massive lherzolite; Mba, metabasalt. (**b**) Typical textural features of the Küre intrusive lherzolite (sample K4b). Rounded olivines (Ol) are included in large diopside (Cpx) and bronzite. (**c**) Microscopic view of the metabasalt at the contact zone with the lherzolite east of Karacakaya tepe (sample K4d). Act, actinolite; Cpx, diopside; İlm, ilmenite; Gr, garnet; (**d**). General microscopic view of the basalt, 20 m from the contact with the lherzolite east of Karacakaya tepe (sample K4e).

In host basalts, along a zone a few metres wide from the lherzolite, high-temperature metamorphic effects are observed. Macroscopically, this zone has a compact aspect and light green colour dotted with dark coloured specks. In thin section, these specks represent unaltered relicts of clinopyroxene (5–8 mm), green hornblende (2–5 mm), garnet (4–6 mm) and aggregates formed by ilmenite and titanite (Figure 4c). This paragenesis corresponds to the pyroxene hornfels facies of Winkler (1975), indicating temperature conditions of greater than 600°C. The altered matrix of basalt is composed of prehnite, chlorite and actinolite. These low temperature minerals are also observed in the veins cross-cutting the rock and probably formed by the breakdown of plagioclase and mafic minerals. The common basalts show microlitic texture and are composed of plagioclase (0.1–0.3 mm), interstitial augite (0.2–0.5 mm), titanite and magnetite (Figure 4d). Chlorite, epidote and quartz are frequent secondary minerals.

The second lherzolite outcrop occurring 320 m north of the first one is surrounded by gabbros. It has a hectometric triangular outcrop; the contacts are not exposed because of the soil cover and dense vegetation. The gabbros occur as large tabular bodies with longest axis trending in a N40°W direction for about 2 km (Figure 2). Their thickness varies between 200 m and 400 m. In the outcrop area, they are generally massive or display weak layering in places. Some nodules of olivine gabbronorite with rounded shape and decimetric size were observed near the contact with the lherzolite.

In thin section, the gabbros have mesocumulate texture and are formed principally of euhedral and subhedral clinopyroxene and plagioclase (andesine–labradorite). They are equigranular rocks and the grain size varies between 0.7 and 2 mm. Minor brown hastingsitic hornblende forms rims around clinopyroxene. Plagioclase is zoned and partially altered to sericite starting from the central part. Olivine, which is generally a rare mineral included in clinopyroxene and plagioclase, is the principal mineral in the nodules. Titanite, magnetite, hematite and ilmenite are accessory minerals.

4. PETROGRAPHY

The lherzolite is generally fresh and displays poikilitic texture. Rounded olivine is enclosed in large crystals of interstitial clinopyroxene and orthopyroxene (Figure 4b). Olivine is the principal mineral forming 45 to 60% of the rock. It is present as subhedral and anhedral grains and there is no evidence of penetrative deformation. The size varies between 0.2 and 1.5 mm. The clinopyroxene is diopside and forms 20–25% of the rock, whereas the orthopyroxene is bronzite and constitute 15–20% of the rock. Pyroxenes are large, interstitial and poikilitic minerals, ranging in size from 0.8 to 4 mm. Amphibole locally forms up to 20% of the rock. Based on electron microprobe analysis, it is characterized by magnesiohastingsite and kaersutite according to Leake *et al.* (1997)'s classification. Amphibole is strongly pleochroic from light to dark brown. It was presumably formed at the rim of clinopyroxenes during a late stage of crystallization (Figure 5a). Chromium spinel, an accessory cumulus phase, occurs as small euhedral and subhedral minerals ($<150\ \mu m$) in olivine and pyroxene. Plagioclase is generally absent in the major part of the lherzolite, but appears towards the border zone (approximately 2 m thick) with the basalts where it becomes the principal constituent of the rock (30–50%). In this zone, plagioclase occurs as euhedral and subhedral cumulus minerals of labradorite composition, 0.5 to 3 mm in size. Some of the plagioclase is zoned and partially transformed to sericite; sericitization starts from the centre of the crystals. Phlogopite is a minor constituent of the lherzolite. It is observed as a small, subhedral mineral developed at the rim of the olivine and orthopyroxene (Figure 5b). It is particularly abundant in the brecciated border zone. Titanite is a rare and small secondary mineral developed at the rim of the clinopyroxenes. Hydrogrossular is a secondary mineral formed by the late alteration of clinopyroxene (Figure 5c) and amphibole (Figure 5a). Rare tremolite and actinolite associated with the chlorite and talc are observed as alteration products of the clinopyroxene and olivine (Figure 5b).

Detailed examination shows that the primary mineral paragenesis of the lherzolite is represented by olivine and chromite as early cumulus phases, with diopside, bronzite and plagioclase as the late igneous minerals. Hornblende and titanite formed during the late stage of crystallization at the expense of clinopyroxene. Serpentine minerals, phlogopite and hydrogrossular are the secondary minerals formed from the olivine, bronzite and diopside. Tremolite, actinolite, chlorite and sericite are the late alteration products.

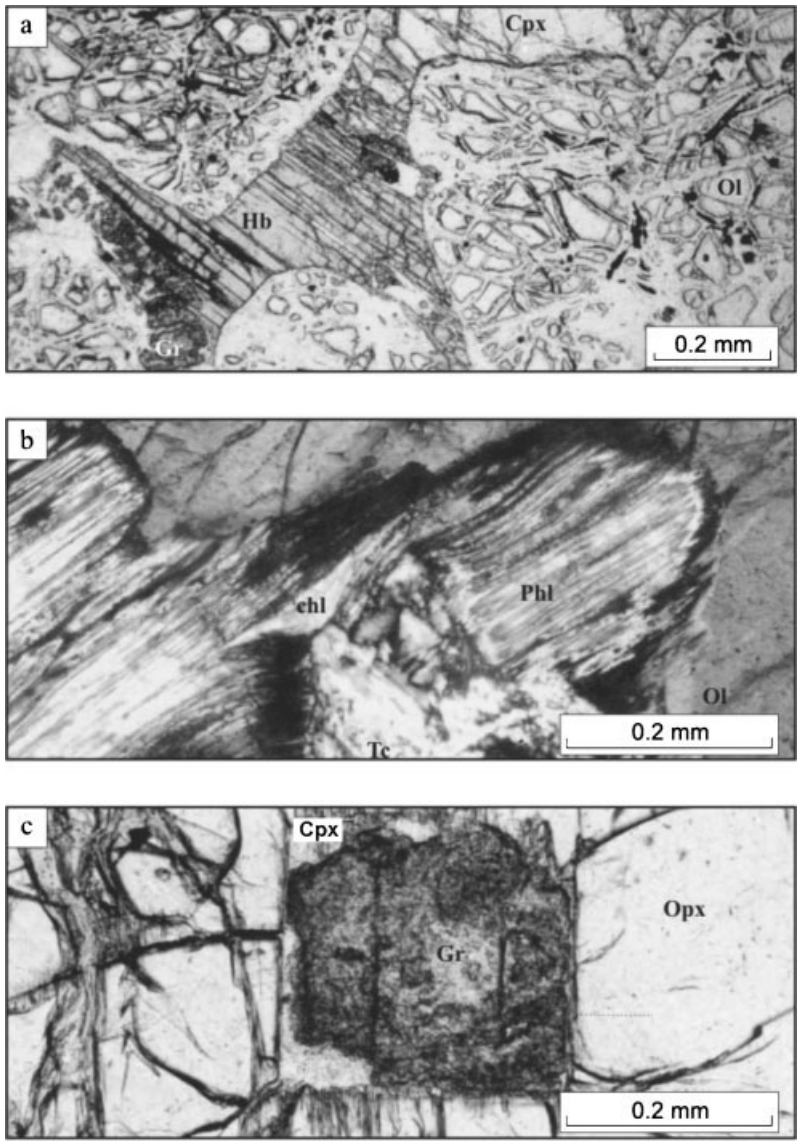

Figure 5. Detailed microscopic views of the intrusive lherzolite. (**a**) Partial transformation of diopside (Cpx) to brown hornblende (Hb) and hydrogrossular (Gr) (sample K25a). (**b**) Transformation of olivine (Ol) to phlogopite (Phl). Late alteration products are represented by talc (Tc) and chlorite (Chl) (sample K25b1). (**c**) Hydrogrossular (Gr) replacing clinopyroxene included in large bronzite (Opx). Radial fractures from garnet indicate that the transformation has occurred by volume augmentation (sample K25b1).

5. CHEMISTRY

5.1. Analytical procedure

The mineral analyses were obtained using JEOL 8900 (CANMET) and Cameca SX 100 instruments at the Technical University of Clausthal. Analytical conditions were 15–20 kV, 20–30 nA and 10–40 seconds peak counting time using wavelength spectrometers.

The whole-rock analyses were performed on a Philips PW-1480 fully automatic X-ray fluorescence spectrometer fitted with a 3.0 kW, 100 kV Rh-anode tube in the Department of Geological Engineering, Hacettepe University, Ankara, Turkey. Major elements were determined on fused glasses prepared with 0.75 g rock powder and 4.5 g lithium tetraborate. The spectrometer was calibrated using international standards (USGS and Geostandards). Corrections were made using Philips software. Matrix effects were compensated for by using Philips' alpha coefficients.

5.2. Whole-rock and mineral chemistry

The whole-rock compositions of five lherzolite samples are given in Table 1. They have approximately similar compositions to the Lewis Hills (Karson *et al.* 1983) and Troodos (Laurent 1992) intrusive lherzolites but with slight enrichment in FeO (Figure 6a, b).

Mineral analyses were performed on two fresh samples (Tables 2 and 3). The first one, K25b1, was taken from the central part of the northern body and the second, K4c, from the brecciated border zone of the southern body, *c.* 20 m from the contact with the basalts (Figures 3 and 4a). The chemical compositions of the primary minerals are in accordance with the intrusive nature of the lherzolites. The olivine is generally homogenous within samples plotting in the layered intrusion field (Figure 7A) defined by Simkin and Smith (1970). Their forsterite content ($Fo_{82–88}$) is significantly lower than the mantle olivine. The majority of the chromium spinels also plot in the field of the layered intrusions and outside the abyssal peridotite field (Figure 7B) (Irvine 1967; Simkin and Smith 1970; Roeder and Campbell 1985).

The primary minerals represent some slight chemical differences between samples. Olivine compositions in sample K25b1, representing the central part of the northern body, vary between 86.3 and 88.1% Fo (Table 2), whereas in sample K4c, taken from the brecciated border zone of the southern body, it is between 81.8 and 83.3% Fo (Table 3). The average NiO contents are 2050–3078 ppm (Tables 2 and 3).

The orthopyroxene ($Wo_{2–3}$ $En_{82–87}$ $Fs_{10–15}$) and clinopyroxene ($Wo_{44–47}$ $En_{48–52}$ $Fs_{4–7}$) show similar variation patterns. Orthopyroxene has the composition of bronzite and contains more magnesium in sample K25b1 (87.12% En) than K4c (83.28% En). Both pyroxenes have approximately equal quantities of TiO_2 in the same sample (Table 2), whereas their average TiO_2 content varies, from sample K25b1 to K4c, from 0.19% to 0.44% in clinopyroxene and 0.18% to 45% in orthopyroxene. Similarly, the average Na_2O content of the clinopyroxenes in sample K25b is 0.15%, whereas it is clearly higher in sample K4c with 0.25% (Tables 2 and 3).

The chromium spinel has a higher Mg, Cr and Al content in the northern body than in the southern body. Amphibole replacing clinopyroxene is calcic and classified, based on Leake *et al.* (1997), as magnesiohastingsite and rarely as kaersutite.

MgO contents of phlogopite are relatively constant with values between 22.26 and 23.47%, whereas Na_2O, K_2O and FeO contents vary from one grain to another (Tables 2 and 3). The average values of $K/K + Na$ and $Mg/Mg + Fe$, are 0.573 and 0.841, respectively; they are low in comparison to the phlogopite of upper mantle peridotites documented by Arai (1984) and Arai and Natsuko (1989). Garnets are determined, based on their optical characteristics, as hydrogrossular and are composed principally of grossular components (Table 3).

6. P–T CONDITIONS

Pressure condition was estimated based on crystal-structure modelling of clinopyroxene for basaltic systems (Nimis 1995). The geobarometer reproduces experimental pressures within ± 2 kbar ($= 1\sigma$; max. error ≤ 5 kb). Mg numbers in sample K25b1 (0.93–0.94) are slightly higher than the limits (0.7–0.9) proposed by Nimis (1995), while Mg numbers in sample K4c (0.87) are within the limits.

The pressures calculated on seven clinopyroxene microanalyses in samples K25b1 and K4c, vary between 0.306 and 1.589 kbar with an average of 0.9 kb (Tables 2 and 3). This average value indicates a depth of *c.* 2.7 km for the crystallization of clinopyroxene.

Table 1. Whole-rock compositions of the Küre lherzolite. Total iron is expressed as Fe_2O_3

	K11	K6a	K4a	K4b	K4c
SiO_2	40.12	40.22	41.02	40.19	42.14
Al_2O_3	4.02	5.31	6.65	4.74	6.33
$Fe_2O_{3\ tot.}$	12.31	13.09	14.36	14.26	12.74
MnO	0.17	0.19	0.21	0.21	0.19
MgO	31.34	31.10	27.41	30.95	26.93
CaO	4.60	3.79	5.43	4.09	6.11
Na_2O	0.24	0.38	0.44	0.45	0.51
K_2O	0.02	0.06	0.07	0.04	0.19
TiO_2	0.21	0.38	0.32	0.27	0.36
P_2O_5	0.00	0.02	0.01	0.01	0.03
H_2O	6.06	4.63	4.81	4.81	3.11
Total	99.10	99.16	100.17	100.02	98.63

The intracrystalline cation partitioning between M1 and M2 sites of clinopyroxene were used to estimate closure temperatures (cf. Molin and Zanazzi 1991). The temperatures calculated from clinopyroxenes in samples K25b1 and K4c vary between 884 and 904°C with an average value of 897°C (Tables 2 and 3).

Temperatures were also calculated using the olivine–spinel Mg–Fe^{2+} exchange thermometer (cf. Ballhaus *et al.* 1991) from the average compositions of olivine and chromite in samples K25b1 and K4c. Estimated temperatures are 1070°C in sample K25b1 and 1015°C in sample K4c (Tables 2 and 3). These are clearly higher than the temperatures calculated by the clinopyroxene geothermometer. This difference is in accordance with the explanation that olivine and chromite represent the early cumulus phases and the clinopyroxene the late poikilitic mineral. Nevertheless, orthopyroxene is also the late poikilitic mineral formed after olivine and chromite and its crystallization temperature must be lower than that of the first cumulus minerals. To test this hypothesis, the equilibration temperature of orthopyroxene was estimated by the method proposed by Lindsley (1983). The average compositions of orthopyroxene yield approximately 900°C for K4c and 950°C for K25b1. Although the uncertainty of this method is as large as ± 50°C, this range of temperature is approximately in accordance with the late crystallization of the orthopyroxene.

In conclusion, chromite and olivine, the early cumulus minerals, were formed at temperatures between 1015 and 1070°C, whereas clinopyroxene and orthopyroxene, the late intercumulus poikilitic minerals, formed at between 900 and 950°C.

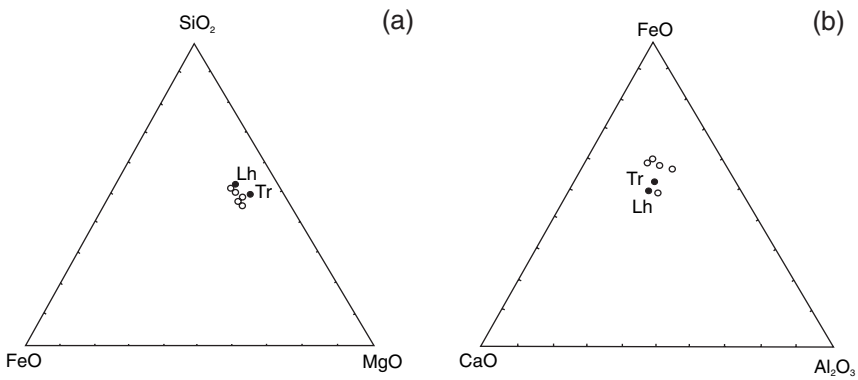

Figure 6. Whole-rock chemical variations of Küre lherzolite on (**a**) SiO_2–MgO–FeO, (**b**) FeO–CaO–Al_2O_3 diagrams. Lh, average composition of the seven intrusive feldspathic lherzolite samples from the Lewis Hills Massif (Karson *et al.* 1983). Tr, average composition of the intrusive poikilitic peridotite from the Troodos Massif (Laurent 1992).

Table 2. Mineral compositions of the Küre lherzolite in sample K25b1. 'Av' indicate the average value

Chromite	1	2	3	4	5	6	7	8	9	10	11	12	13	14		Av. chr
SiO_2	0.03	0.02	0.01	0.02	0.03	0.06	0.01	0.03	0.01	0.03	0.04	0.03	0.04	0.00	SiO_2	0.02
TiO_2	3.05	2.94	3.38	3.33	2.15	0.56	0.61	0.62	2.11	2.16	2.01	2.64	2.72	2.69	TiO_2	1.97
Al_2O_3	12.48	12.58	11.90	11.76	14.70	15.27	17.98	18.23	14.94	14.99	14.90	13.31	13.16	12.78	Al_2O_3	14.19
Cr_2O_3	35.98	35.74	35.63	35.42	36.05	40.39	45.08	44.18	35.83	35.63	35.61	38.38	38.09	37.96	Cr_2O_3	38.96
V_2O_3	0.58	0.54	0.52	0.50	0.47	0.39	0.35	0.36	0.48	0.45	0.45	0.45	0.52	0.53	V_2O_3	0.44
Fe_2O_3	15.84	15.87	16.16	16.26	14.97	12.46	7.28	7.44	15.62	15.40	15.24	13.67	14.04	14.25	Fe_2O_3	13.17
FeO	23.37	22.88	23.63	23.47	22.64	20.82	17.35	17.28	22.39	22.32	22.16	21.91	21.92	21.60	FeO	21.55
MnO	0.42	0.42	0.41	0.43	0.42	0.41	0.34	0.33	0.39	0.42	0.41	0.37	0.38	0.39	MnO	0.40
MgO	8.13	8.29	8.09	8.00	8.26	8.47	11.54	11.51	8.62	8.58	8.48	9.00	9.01	9.05	MgO	8.86
NiO	0.26	0.25	0.23	0.25	0.24	0.13	0.17	0.18	0.21	0.23	0.21	0.23	0.26	0.26	NiO	0.20
ZnO	0.18	0.15	0.17	0.20	0.24	0.23	0.21	0.08	0.20	0.20	0.15	0.11	0.14	0.09	ZnO	0.16
Total	100.32	99.68	100.13	99.64	100.17	99.19	100.92	100.24	100.80	100.41	99.66	100.10	100.28	99.60	Total	99.92
No. of oxygen 4																
Si	0.001	0.001	0.000	0.001	0.001	0.002	0.000	0.001	0.000	0.001	0.001	0.001	0.001	0.000	Si	0.0007
Ti	0.080	0.078	0.089	0.089	0.056	0.014	0.015	0.015	0.054	0.056	0.052	0.068	0.070	0.070	Ti	0.0511
Al	0.515	0.521	0.494	0.491	0.598	0.619	0.682	0.695	0.604	0.607	0.608	0.540	0.534	0.523	Al	0.5736
Cr	0.995	0.993	0.991	0.992	0.984	1.098	1.147	1.129	0.972	0.969	0.975	1.044	1.037	1.042	Cr	1.0562
V	0.016	0.015	0.015	0.014	0.013	0.011	0.009	0.009	0.013	0.012	0.012	0.012	0.014	0.015	V	0.0121
Fe^{+3}	0.417	0.420	0.428	0.433	0.389	0.322	0.176	0.181	0.403	0.398	0.397	0.354	0.364	0.372	Fe^{+3}	0.3416
Fe^{+2}	0.683	0.672	0.695	0.695	0.654	0.598	0.467	0.467	0.642	0.642	0.642	0.630	0.631	0.627	Fe^{+2}	0.6200
Mn	0.012	0.013	0.012	0.013	0.012	0.012	0.009	0.009	0.011	0.012	0.012	0.011	0.011	0.011	Mn	0.0116
Mg	0.424	0.434	0.424	0.422	0.425	0.434	0.554	0.555	0.441	0.440	0.438	0.462	0.462	0.469	Mg	0.4522
Ni	0.007	0.007	0.007	0.007	0.007	0.004	0.004	0.005	0.006	0.006	0.006	0.006	0.007	0.007	Ni	0.0056
Zn	0.005	0.004	0.004	0.005	0.006	0.006	0.003	0.002	0.005	0.005	0.004	0.003	0.004	0.002	Zn	0.0042
Total	3.155	3.158	3.159	3.162	3.145	3.120	3.066	3.068	3.151	3.148	3.147	3.131	3.135	3.138	Total	3.1289
XMg1	0.278	0.285	0.274	0.272	0.290	0.320	0.463	0.461	0.297	0.297	0.297	0.319	0.317	0.319	XspCr	0.6483
XMg2	0.383	0.392	0.379	0.378	0.394	0.420	0.543	0.543	0.407	0.407	0.406	0.423	0.423	0.428	$XspFe^{+3}$	0.3551
YCr	0.517	0.514	0.518	0.518	0.499	0.538	0.572	0.563	0.491	0.491	0.492	0.539	0.536	0.538	$XspFe^{+2}$	0.5748
XCr	0.659	0.656	0.668	0.669	0.622	0.640	0.627	0.619	0.617	0.615	0.616	0.659	0.660	0.666	XspAl	0.2910
XNi	0.006	0.006	0.006	0.006	0.006	0.003	0.004	0.005	0.005	0.006	0.005	0.006	0.006	0.007	XspMg	0.4252
XZn	0.004	0.003	0.004	0.005	0.006	0.006	0.003	0.002	0.005	0.005	0.003	0.003	0.003	0.002		
															T^0C	1070
															fO_2	3.51

Table 2. *Continues*

Table 2. *Continued*

Olivine	15	16	17	18	19	20	21	22	23	Av. olivine
SiO_2	39.65	39.67	40.19	40.40	40.07	40.19	40.37	39.89	39.92	40.04
TiO_2	0.02	0.02	0.01	0.00	0.00	0.00	0.00	0.01	0.02	0.01
Al_2O_3	0.01	0.00	0.04	0.00	0.03	0.00	0.01	0.00	0.01	0.01
Cr_2O_3	0.01	0.00	0.01	0.02	0.00	0.02	0.02	0.01	0.00	0.01
FeO	13.30	13.30	11.95	12.02	13.15	13.29	12.89	12.68	11.64	12.69
MnO	0.21	0.19	0.19	0.18	0.20	0.21	0.20	0.18	0.18	0.19
MgO	46.97	47.24	47.55	47.84	46.76	47.02	46.71	47.36	48.20	47.29
CaO	0.03	0.04	0.04	0.02	0.07	0.07	0.05	0.03	0.03	0.04
Na_2O	0.00	0.00	0.00	0.00	0.00	0.00	0.00	0.00	0.00	0.00
NiO	0.29	0.32	0.32	0.29	0.31	0.29	0.31	0.32	0.32	0.31
Total	100.49	100.78	100.30	100.77	100.59	101.09	100.56	100.48	100.32	100.59
No. of oxygen 4										
Si	0.985	0.983	0.994	0.994	0.993	0.992	0.999	0.988	0.986	0.988
Ti	0.000	0.000	0.000	0.000	0.000	0.000	0.000	0.000	0.000	0.000
Al	0.000	0.000	0.001	0.000	0.001	0.000	0.000	0.000	0.000	0.000
Cr	0.000	0.000	0.000	0.000	0.000	0.000	0.000	0.000	0.000	0.000
Fe	0.276	0.276	0.247	0.247	0.273	0.274	0.267	0.263	0.240	0.261
Mn	0.004	0.004	0.004	0.004	0.004	0.004	0.004	0.004	0.004	0.004
Mg	1.740	1.745	1.752	1.754	1.728	1.730	1.723	1.749	1.775	1.751
Ca	0.001	0.001	0.001	0.001	0.002	0.002	0.001	0.001	0.001	0.001
Na	0.000	0.000	0.000	0.000	0.000	0.000	0.000	0.000	0.000	0.000
Ni	0.006	0.006	0.006	0.006	0.006	0.006	0.006	0.006	0.006	0.006
Total	3.012	3.015	3.005	3.006	3.007	3.008	3.000	3.011	3.012	3.012
XMg	0.863	0.864	0.879	0.876	0.864	0.863	0.866	0.869	0.881	0.870

Table 2. *Continues*

Orthopyroxene

	24	25	26	27	28	29		Av. opx.	Clinopyroxene	30	31	32	33	34	Amphibole	35	36	Av. Amph
SiO_2	55.84	56.08	56.23	56.25	55.22	55.76	SiO_2	55.91	SiO_2	53.61	53.23	52.62	52.46	52.59	SiO_2	43.61	43.75	43.7
TiO_2	0.13	0.11	0.08	0.12	0.28	0.36	TiO_2	0.18	TiO_2	0.14	0.16	0.17	0.25	0.25	TiO_2	3.69	3.84	3.77
Al_2O_3	1.39	1.52	1.24	1.44	1.21	1.16	Al_2O_3	1.33	Al_2O_3	1.62	1.95	2.29	0.24	2.12	Al_2O_3	10.17	10.38	10.3
Cr_2O_3	0.47	0.44	0.38	0.46	0.32	0.30	Cr_2O_3	0.40	Cr_2O_3	0.75	0.90	1.09	0.78	0.83	Cr_2O_3	1.38	1.35	1.37
FeO	7.49	7.43	7.38	7.21	8.36	8.27	FeO	7.69	FeO	3.11	3.30	3.23	3.57	3.61	Fe_2O_3	2.62	1.82	2.22
MnO	0.20	0.19	0.19	0.20	0.22	0.21	MnO	0.20	MnO	0.11	0.11	0.13	0.12	0.09	FeO	3.24	4.06	3.65
MgO	32.54	32.69	32.76	32.49	32.63	32.60	MgO	32.62	MgO	17.49	18.42	18.07	18.05	18.04	MnO	0.08	0.08	0.08
CaO	1.53	1.52	1.56	1.58	0.99	1.01	CaO	1.37	CaO	23.05	21.62	21.99	21.77	21.72	MgO	16.98	16.74	16.9
Na_2O	0.01	0.00	0.01	0.01	0.02	0.01	Na_2O	0.01	Na_2O	0.22	0.17	0.12	0.12	0.12	NiO	0.08	0.10	0.09
K_2O	0.00	0.00	0.00	0.00	0.00	0.00	K_2O	0.00	K_2O	0.00	0.00	0.00	0.00	0.00	ZnO	0.00	0.02	0.01
Total	99.60	99.98	99.83	99.76	99.25	99.68	Total	99.71	Total	100.10	99.86	99.71	97.36	99.37				
Si	1.954	1.953	1.961	1.961	1.946	1.954			Si	1.945	1.931	1.914	1.915	1.925	CaO	11.57	11.62	11.6
Ti	0.003	0.003	0.002	0.003	0.007	0.009			Ti	0.004	0.004	0.005	0.007	0.007	Na_2O	2.61	2.67	2.64
Al	0.057	0.062	0.051	0.059	0.050	0.048	Si	1.9515	Al	0.069	0.083	0.098	0.096	0.091	K_2O	0.14	0.14	0.14
Cr	0.013	0.012	0.010	0.013	0.009	0.008	TiIV	0.0000	Cr	0.022	0.026	0.313	0.023	0.024	H_2O	2.07	2.07	2.07
Fe	0.219	0.216	0.215	0.210	0.246	0.242	TiVI	0.0047	Fe^{2+}	0.070	0.070	0.060	0.065	0.074	Total	98.24	98.64	98.5
Mn	0.006	0.006	0.006	0.006	0.007	0.006	AlIV	0.0485	Fe^{3+}	0.024	0.030	0.038	0.044	0.036				
Mg	1.697	1.697	1.703	1.688	1.714	1.703	AlVI	0.0061	Mn	0.003	0.003	0.004	0.004	0.003	No.of oxygen 23			
Ca	0.057	0.057	0.058	0.059	0.037	0.038	Cr	0.0110	Mg	0.952	1.002	0.986	0.988	0.988	Si	6.327	6.332	6.33
Na	0.001	0.000	0.001	0.001	0.001	0.001	Fe^{2+}	0.2014	Ca	0.896	0.840	0.857	0.852	0.850	AlIV	1.673	1.668	1.67
K	0.000	0.000	0.000	0.000	0.000	0.000	Fe^{3+}	0.0223	Na	0.015	0.012	0.008	0.009	0.009	AlVI	0.067	0.103	0.09
Total	4.007	4.006	4.007	4.000	4.017	4.009	Mn	0.0059	K	0.000	0.000	0.000	0.000	0.000	Ti	0.403	0.418	0.41
							Mg	1.7079	Total	4.000	4.001	4.283	4.001	4.006	Cr	0.158	0.154	0.16
															Fe^{3+}	0.286	0.198	0.24
XMgt	0.886	0.887	0.888	0.889	0.874	0.875	Ca	0.0512	Alt	0.055	0.069	0.086	0.085	0.080	Fe^{2+}	0.393	0.492	0.44
AlIV	0.046	0.047	0.039	0.039	0.050	0.046	Na	0.0003	AlM1	0.014	0.014	0.012	0.011	0.012	Mn	0.009	0.010	0.01
AlVI	0.011	0.016	0.012	0.020	0.000	0.002	K	0.0003	$Fe^{2+}M1$	0.046	0.035	0.031	0.033	0.036	Mg	3.673	3.361	3.52
Fe^{2+}	0.203	0.203	0.202	0.210	0.218	0.224	Total	4.0111	$Fe^{2+}M2$	0.023	0.034	0.028	0.031	0.037	Ni	0.010	0.012	0.01
Fe^{3+}	0.016	0.013	0.014	0.000	0.028	0.018			MgM1	0.890	0.891	0.883	0.883	0.886	Zn	0.000	0.002	0
XmMg	0.893	0.893	0.894	0.889	0.887	0.884	En	0.8712	MgM2	0.062	0.111	0.103	0.105	0.102	Ca	1.798	1.802	1.8
En	0.867	0.867	0.868	0.863	0.870	0.867	Fo	0.1027	R^{3+}	0.064	0.074	0.086	0.084	0.078	Na	0.733	0.748	0.74
Fs	0.104	0.104	0.103	0.107	0.111	0.114	Wo	0.0261	CNM	0.915	0.855	0.869	0.864	0.861	K	0.025	0.025	0.03
Wo	0.029	0.029	0.030	0.030	0.019	0.019			Kd	0.131	0.129	0.130	0.129	0.129	Total	15.555	15.325	15.4
XMgM1	0.854	0.854	0.860	0.857	0.848	0.850			P(kbar)	0.306	0.892	0.556	0.987	0.608				
XFeM1	0.102	0.102	0.102	0.106	0.108	0.112			T^0C	901.5	901.3	903.8	900.9	888.8				
XMgM2	0.836	0.838	0.837	0.831	0.848	0.844												
XFeM2	0.100	0.100	0.099	0.103	0.108	0.111												
XCaM2	0.057	0.056	0.058	0.059	0.037	0.038												

Table 3. Mineral compositions of the Küre lherzolite in sample K4c. 'Av' indicate the average value

Chromite	1	2	3	4	5	6	7	8	9	10	11	12	13		Av. chr
SiO_2	0.04	0.02	0.01	0.02	0.02	0.00	0.02	0.02	0.02	0.02	0.02	0.03	0.38	SiO_2	0.05
TiO_2	6.76	3.76	0.45	1.07	1.76	2.02	7.60	7.29	5.70	5.59	5.44	1.41	0.98	TiO_2	3.83
Al_2O_3	8.53	7.14	13.94	12.31	10.98	12.57	8.78	8.34	8.79	6.98	7.23	13.23	12.21	Al_2O_3	10.08
Cr_2O_3	23.76	20.59	34.02	35.56	34.62	29.37	24.76	24.18	25.40	23.44	23.14	35.98	29.53	Cr_2O_3	28.03
V_2O_3	0.76	0.56	0.36	0.38	0.32	0.36	0.72	0.59	0.58	0.70	0.73	0.36	0.27	V_2O_3	0.51
Fe_2O_3	24.27	32.45	19.40	18.99	20.03	22.65	21.39	23.17	24.80	27.81	27.77	16.50	24.24	Fe_2O_3	23.34
FeO	28.05	30.67	24.47	24.65	26.53	26.37	29.44	28.17	27.59	30.34	30.01	25.38	25.23	FeO	27.45
MnO	0.43	0.39	0.46	0.43	0.43	0.41	0.49	0.40	0.40	0.46	0.48	0.44	0.41	MnO	0.43
MgO	6.68	2.80	5.81	6.06	5.17	5.42	6.34	6.88	6.56	4.35	4.39	5.79	5.31	MgO	5.50
NiO	0.26	0.24	0.14	0.12	0.15	0.18	0.23	0.23	0.14	0.26	0.23	0.15	0.09	NiO	0.19
ZnO	0.06	0.13	0.22	0.16	0.13	0.14	0.08	0.08	0.08	0.11	0.14	0.20	0.19	ZnO	0.13
Total	99.59	98.75	99.28	99.75	100.14	99.49	99.85	99.35	100.07	100.06	99.59	99.48	98.84	Total	99.54
No. of oxygen 4															
Si	0.0020	0.0010	0.0000	0.0010	0.0010	0.0010	0.0010	0.0010	0.0010	0.0010	0.0010	0.0010	0.0140	Si	0.0017
Ti	0.1900	0.1150	0.0120	0.0290	0.0490	0.0560	0.2120	0.2150	0.1600	0.1630	0.1600	0.0380	0.0280	Ti	0.0995
Al	0.3770	0.3430	0.5950	0.5250	0.4750	0.5470	0.3830	0.3680	0.3870	0.3200	0.0320	0.5590	0.5380	Al	0.4110
Cr	0.7040	0.6630	0.9740	1.0170	1.0040	0.8580	0.7250	0.7150	0.7510	0.7210	0.7140	1.0200	0.8730	Cr	0.7670
V	0.0230	0.0180	0.0100	0.0110	0.0090	0.0110	0.0210	0.0180	0.0170	0.0220	0.0230	0.0100	0.0080	V	0.0140
Fe^{+3}	0.6840	0.9940	0.5280	0.5170	0.5530	0.6290	0.5960	0.6520	0.6980	0.8130	0.8150	0.4450	0.6820	Fe^{+3}	0.6066
Fe^{+2}	0.8790	1.0440	0.7410	0.7460	0.8130	0.8140	0.9110	0.8810	0.8620	0.9860	0.9790	0.7610	0.7890	Fe^{+2}	0.7926
Mn	0.0140	0.0130	0.0140	0.0130	0.0130	0.0130	0.0150	0.0130	0.0130	0.0150	0.0160	0.0130	0.0130	Mn	0.0126
Mg	0.3730	0.1700	0.3130	0.3270	0.2890	0.2980	0.3500	0.3840	0.3660	0.2520	0.2550	0.3090	0.2960	Mg	0.2860
Ni	0.0080	0.0080	0.0040	0.0030	0.0040	0.0050	0.0070	0.0070	0.0040	0.0080	0.0070	0.0040	0.0030	Ni	0.0053
Zn	0.0020	0.0040	0.0060	0.0040	0.0040	0.0040	0.0020	0.0020	0.0020	0.0030	0.0040	0.0050	0.0050	Zn	0.0032
Total	3.2560	3.3730	3.1970	3.1930	3.2140	3.2360	3.2230	3.2560	3.2610	3.3040	3.0060	3.1650	3.2490	Total	2.9995
XMg1	0.1930	0.0770	0.1980	0.2060	0.1710	0.1710	0.1880	0.2000	0.1900	0.1230	0.1250	0.2040	0.1680	XspCr	0.6510
XMg2	0.2980	0.1400	0.2970	0.3050	0.2580	0.2680	0.2770	0.3030	0.2980	0.2040	0.2070	0.2890	0.2730	$XspFe^{+3}$	0.4335
YCr	0.3990	0.3320	0.4640	0.4940	0.4940	0.4220	0.4250	0.4120	0.4090	0.3890	0.3830	0.5040	0.4170	$XspFe^{+2}$	0.7348
XCr	0.6520	0.6590	0.6210	0.6600	0.6790	0.6110	0.6540	0.6600	0.6600	0.6930	0.6820	0.6460	0.6190	XspAl	0.2303
XNi	0.0060	0.0060	0.0040	0.0030	0.0040	0.0050	0.0050	0.0050	0.0030	0.0060	0.0060	0.0040	0.0020	XspMg	0.2652
XZn	0.0010	0.0030	0.0050	0.0040	0.0030	0.0030	0.0020	0.0020	0.0020	0.0020	0.0030	0.0050	0.0050		
														T^0C	1015
														fO_2	3.43

Table 3. *Continues*

Table 3. *Continued*

Olivine	14	15	16	17	18	19	20	21	22	23	Av. ol.
SiO_2	39.54	39.25	39.75	39.22	38.45	39.11	39.11	39.90	39.57	39.51	39.34
TiO_2	0.02	0.03	0.01	0.00	0.04	0.02	0.01	0.00	0.01	0.02	0.01
Al_2O_3	0.01	0.00	0.02	0.00	0.00	0.01	0.00	0.00	0.01	0.00	0.01
Cr_2O_3	0.01	0.01	0.01	0.00	0.02	0.03	0.01	0.01	0.05	0.02	0.02
FeO	17.09	17.17	16.70	16.27	16.93	17.02	16.00	16.14	16.75	16.78	16.69
MnO	0.27	0.26	0.26	0.28	0.03	0.27	0.25	0.26	0.26	0.28	0.27
MgO	43.40	43.42	43.89	44.24	43.76	44.10	44.72	44.77	44.11	44.09	44.05
CaO	0.07	0.05	0.06	0.07	0.09	0.07	0.06	0.05	0.10	0.08	0.07
Na_2O	0.00	0.00	0.00	0.00	0.01	0.01	0.00	0.00	0.00	0.01	0.00
NiO	0.23	0.22	0.19	0.17	0.19	0.20	0.19	0.21	0.22	0.23	0.21
Total	100.64	100.41	100.89	100.25	99.52	100.84	100.35	101.34	101.08	101.02	100.67
No. of oxygen 4											
Si	0.997	0.993	0.998	0.990	0.980	0.985	0.986	0.994	0.992	0.992	0.989
Ti	0.000	0.001	0.000	0.000	0.001	0.000	0.000	0.000	0.000	0.000	0.000
Al	0.000	0.000	0.001	0.000	0.000	0.000	0.000	0.000	0.000	0.000	0.000
Cr	0.000	0.000	0.000	0.000	0.001	0.000	0.000	0.000	0.001	0.000	0.000
Fe	0.360	0.363	0.351	0.344	0.361	0.359	0.337	0.336	0.351	0.352	0.350
Mn	0.006	0.006	0.006	0.006	0.006	0.006	0.005	0.005	0.006	0.006	0.006
Mg	1.631	1.638	1.642	1.665	1.663	1.656	1.680	1.663	1.649	1.650	1.660
Ca	0.002	0.001	0.002	0.002	0.002	0.002	0.002	0.001	0.003	0.002	0.002
Na	0.000	0.000	0.000	0.000	0.000	0.000	0.000	0.000	0.000	0.001	0.004
Ni	0.005	0.004	0.004	0.003	0.004	0.004	0.004	0.004	0.005	0.005	0.000
Total	3.001	3.006	3.004	3.010	3.018	3.012	3.014	3.003	3.007	3.008	3.011
XMg	0.819	0.818	0.824	0.829	0.822	0.822	0.833	0.832	0.824	0.824	0.826

Table 3. *Continued*

Orthopyroxene	24	25	26	27	28	Av. Opx		Clinopyroxene	29	30
SiO_2	55.02	54.72	54.75	55.16	55.47	55.02		SiO_2	51.69	52.03
TiO_2	0.46	0.43	0.49	0.49	0.36	0.45		TiO_2	0.44	0.43
Al_2O_3	1.43	1.18	1.20	1.37	1.02	1.24		Al_2O_3	2.94	2.90
Cr_2O_3	0.28	0.25	0.28	0.30	0.22	0.27		Cr_2O_3	1.07	1.09
FeO	10.12	10.10	10.78	10.43	10.54	10.39		FeO	4.63	4.77
MnO	0.26	0.27	0.27	0.27	0.28	0.27		MnO	0.12	0.15
MgO	30.59	30.96	30.80	31.05	31.03	30.89		MgO	16.44	16.65
CaO	1.37	1.23	1.19	1.14	1.10	1.21		CaO	21.38	21.13
Na_2O	0.02	0.02	0.02	0.02	0.02	0.02		Na_2O	0.24	0.25
K_2O	0.00	0.00	0.00	0.00	0.00	0.00		K_2O	0.00	0.00
Total	99.55	99.16	99.78	100.23	100.04	99.76		Total	98.95	99.40
Si	1.949	1.947	1.942	1.943	1.957			No of oxygen 6		
Ti	0.012	0.012	0.013	0.013	0.010	No of oxygen 6		Si	1.9088	1.9122
Al	0.060	0.049	0.050	0.057	0.042	Si	1.9458	Ti	0.0120	0.0119
Cr	0.008	0.007	0.008	0.008	0.006	TiIV	0.0260	Al	0.1277	0.1254
Fe	0.300	0.301	0.320	0.307	0.311	TiVI	0.0093	Cr	0.0312	0.0316
Mn	0.008	0.008	0.008	0.008	0.008	AlIV	0.0516	Fe^{2+}	0.1290	0.1323
Mg	1.615	1.642	1.629	1.630	1.632	AlVI	0.0000	Fe^{3+}	0.0148	0.0138
Ca	0.052	0.047	0.045	0.043	0.042	Cr	0.0113	Mn	0.0037	0.0047
Na	0.001	0.001	0.001	0.001	0.001	Fe^{2+}	0.2831	Mg	0.9106	0.9179
K	0.000	0.000	0.000	0.000	0.000	Fe^{3+}	0.0231	Ca	0.8460	0.8320
Total	4.005	4.014	4.016	4.010	4.009	Mn	0.0080	Na	0.0170	0.1780
						Mg	1.6387	K	0.0000	0.0000
XMgt	0.843	0.845	0.836	0.841	0.840	Ca	0.0458	Total	4.0008	4.1598
AlIV	0.051	0.049	0.050	0.057	0.042	Na	0.0014			
AlVI	0.009	0.000	0.000	0.000	0.000	K	0.0000	Alt	0.0912	0.0878
Fe^{2+}	0.289	0.280	0.302	0.284	0.292	Total	4.0441	AlM1	0.0365	0.0376
Fe^{3+}	0.011	0.021	0.018	0.024	0.019			Fe^{2+}M1	0.0741	0.0736
XmMg	0.848	0.854	0.843	0.852	0.848	En	0.8328	Fe^{2+}M2	0.0541	0.0591
En	0.826	0.834	0.824	0.833	0.830	Fo	0.1439	MgM1	0.8320	0.8315
Fs	0.148	0.142	0.153	0.145	0.149	Wo	0.0232	MgM2	0.0792	0.0865
Wo	0.027	0.024	0.023	0.022	0.021			R^{3+}	0.0945	0.0949
XMgM1	0.814	0.821	0.811	0.813	0.819			CNM	0.8667	0.8545
XFeM1	0.146	0.140	0.151	0.142	0.147			Kd	0.1298	0.1293
XMgM2	0.797	0.807	0.798	0.808	0.805			P(kbar)	1.313	1.589
XFeM2	143.000	0.137	0.148	0.141	0.144					
XCaM2	0.052	0.046	0.044	0.043	0.041					

7. OXYGEN FUGACITY

An important source of information on the geodynamic environment of the mantle-derived melts is the oxygen fugacity. Application of the oxygen barometer to the mantle and mantle-derived rocks (cf. Ballhaus *et al.* 1991) reveals that abyssal peridotites, MORBs, and peridotite xenolites in the undepleted fertile mantle and depleted mid-oceanic ridge regions were generated in reduced environments ($\Delta\log fO_2 < +1$), whereas cumulate inclusions in arc basalts, as well as Alaskan-type intrusives, have higher degrees of oxygen fugacity ($\Delta\log fO_2 > +1$, generally around $+2$). Mattioli *et al.* (1989) interpreted the high degree of fO_2 of the upper mantle rocks as resulting from oxidation of the mantle minerals by CO_2–H_2O rich fluids derived from the subducted material.

The values of $\Delta\log (fO_2)$, calculated from the average compositions of olivine and chromite minerals according to the semi-empirical oxygen geobarometer of Ballhaus *et al.* (1991) in samples K25 b1 and K4c, are 3.51 and 3.43 log units, respectively (Tables 2 and 3). High oxygen fugacity values obtained from the Küre lherzolite indicate an origin in an oxidizing arc environment.

8. PETROLOGICAL INTERPRETATION OF THE KÜRE LHERZOLITE

The presence of late ultramafic–mafic intrusive bodies in oceanic crustal sequences has been described for three well-studied ophiolites: the Lewis Hills Massif of western Newfoundland (Karson *et al.* 1983), the Semail ophiolite in Oman (Smewing 1980; Browning and Smewing 1981; Lippard *et al.* 1986; Benn *et al.* 1988; Juteau *et al.* 1988) and the Troodos Massif in Cyprus (Benn and Laurent 1987; Laurent 1992). In these ophiolites, lherzolites, wehrlites and olivine gabbros are the dominant intrusive lithologies with rare dunites, pyroxenites and websterites. These rocks cut the layered cumulate sequences consisting principally of gabbros. Only in the Semail ophiolite can some picritic dykes radiating from the uppermost intrusion be traced up to the upper extrusives (Juteau *et al.* 1988). Poikilitic texture with rounded olivine included in large clinopyroxene and orthopyroxene is the common characteristic of these rocks. Frequently, amphibole and plagioclase are present as interstitial phases (Laurent 1992). By comparison with these massifs, Girardeau and Mercier (1992) have considered the plagioclase–lherzolite cored at site 334 of DSDP Leg 37 on the mid-Atlantic ridge, as the late intrusive rocks in the high-level crustal gabbros.

The formation and rise of late ultrabasic–basic magma within the crustal sequences were partly explained in relation to their geodynamic environment. In the Lewis Hills Massif of western Newfoundland, Karson *et al.* (1983) suggested that the peridotite bodies were emplaced as crystal mushes derived from mobilized ultramafic cumulates along oceanic fracture zones. In the Semail ophiolite, Juteau *et al.* (1988) proposed that the wehrlitic series were rooted in the transitional and impregnated dunites that developed in the uppermost part of the mantle. In the Troodos ophiolite, Laurent (1992) suggested that the parental magma of the intrusive peridotites consisted of an extensively melted peridotite fraction with an additional basaltic magma generated at the uppermost part of a mantle diapir in a suprasubduction zone environment.

The intrusive lherzolite in the Küre ophiolite appears to support Laurent's (1992) hypothesis. From the field and geochemical data, it is generally accepted that the Küre ophiolite represents the fragments of the suprasubduction marginal basin. According to Ustaömer and Robertson (1994, 1999) and Boztuğ *et al.* (1995) the Küre Basin was opened on the northwardly subducted Palaeotethyan oceanic lithosphere where the ophiolites of Elekdağ (Ustaömer and Robertson 1994, 1999) or Çangaldağ (Yilmaz and Boztuğ 1986) represent the remnants. Nevertheless, new radiometric ages (*c.* 100 Ma) of Domuzdağ high pressure metamorphic rocks associated with the Elekdağ ophiolites (Okay *et al.* 2005) require a re-evaluation of the Palaeotethyan hypothesis. In their work, Okay *et al.* (2005) concluded that the northward subduction of the Neotethys, generally believed to have started in the Senonian, was older.

Since there is a continuing debate on the distinction between Palaeotethys and Neotethys, we prefer to use the term 'Tethyan oceanic lithosphere' for the subducted oceanic slab. By Tethys, we infer the ocean that opened in Anatolia in the Late Triassic and closed during Maastrichtian–Late Palaeocene time.

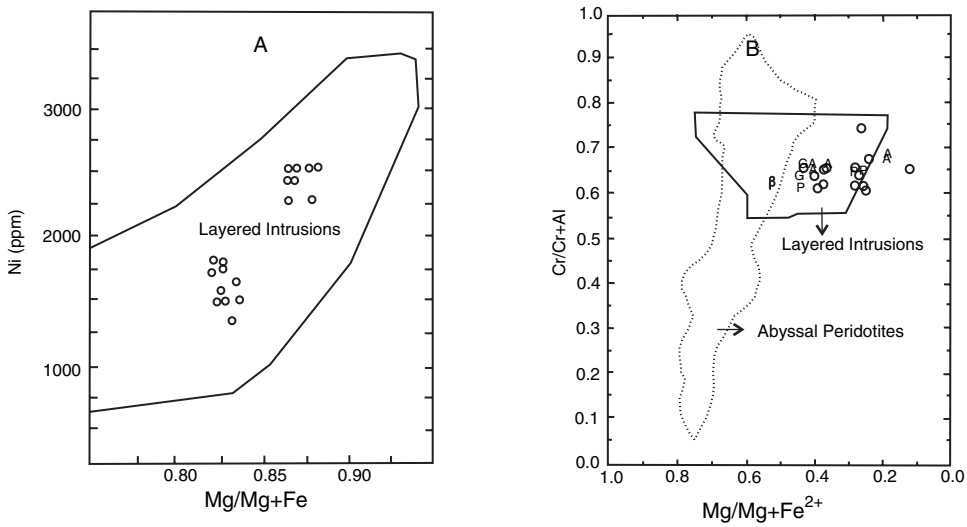

Figure 7. Olivine (**A**) and chromium spinel (**B**) compositions on petrological discrimination diagrams. Letters indicate the host phases of chromium spinels. A, amphibole; G, garnet; O, olivine; P, pyroxene. Dotted line defines the field for abyssal peridotites (Dick and Bullen 1984) and solid line defines the field for layered intrusions (Irvine 1967; Simkin and Smith 1970; Roeder and Campbell 1985).

The schematic illustration about the intrusion of Küre lherzolite within Küre oceanic lithosphere is represented in Figure 8. At latest Triassic time, Tethyan oceanic lithosphere was subducted under the Laurasian margin represented by volcanic-sedimentary series (radiolaritic series or coloured mélange) and Karakaya formations (e.g. Beccaletto and Jenny 2004; Göncüoğlu *et al.* 2004; Okay and Altıner 2004; Pickett and Robertson 2004; Okay and Göncüoğlu 2004; Turhan *et al.* 2004) creating the rifting of the Küre Basin (Figure 8A). The Küre ocean was opened during Early Jurassic, and in the Middle Jurassic Küre lherzolite and gabbro were intruded into Küre oceanic crust (Figure 8B).

The presence of the intrusive lherzolite in such a geological environment reveals some relationships between the generation and rise of the Mg-rich basaltic magma and the subduction event. The principal role of subduction seems to be a mechanism for the introduction of hydrous fluid into the root zones. Hydrous fluids can promote not only the extensive melting of the upper mantle by lowering its solidus temperature, but also help the parental magma to rise within the crustal sequences because of density differences. In the Küre and Troodos ophiolites, the presence of amphibole in the intrusive peridotites indicates the existence of hydrous fluids during cooling of the magma. High oxygen fugacity values of the Küre lherzolite provide additional support for an origin of oxidized arc basaltic magma.

Another common characteristic of the late intrusive peridotites is their poikilitic texture with subhedral and anhedral rounded olivine included in large pyroxenes. Amphibole is the other frequent interstitial phase. In Troodos and Semail intrusive peridotites, olivine grains exhibiting kink-bands are interpreted as mantle xenocrysts (Laurent 1992; Juteau *et al.* 1988). According to Laurent (1992), the poikilitic texture of the Troodos intrusive peridotites implies that the magma was a mixture of liquid and crystals.

In agreement with this hypothesis, the poikilitic texture of the Küre lherzolite is interpreted as the result of crystal mush intrusion. Olivine and chromite were carried as suspended crystals by the magma from which orthopyroxene and clinopyroxene crystallized later. However, unlike these massifs, the olivine grains of the Küre lherzolites do not show traces of penetrative deformation. They often include small euhedral chromite. It is therefore suggested that olivine and the chromite of the Küre intrusive lherzolites represent early cumulus minerals crystallized from the parental magma and carried as suspended crystals. The crystallization temperature of the olivine and chromites is estimated to be between 1015 and 1070°C, and that of the pyroxenes between 897 and

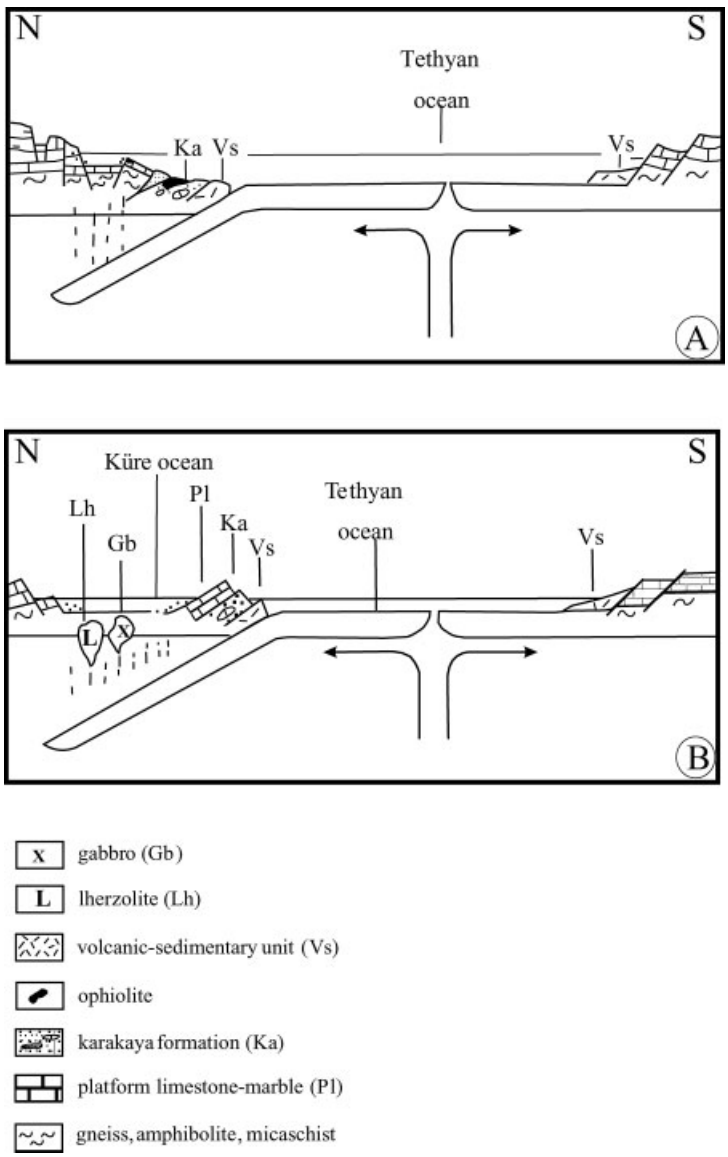

Figure 8. Geodynamical interpretation of the Küre intrusive lherzolite. (**A**) Rifting of the Küre Basin at late Late Triassic time. (**B**) Opening of the Küre ocean in Lower Jurassic and intrusion of the Küre lherzolite and gabbro in Middle Jurassic time.

950°C. The solidification of the magma was completed in the lower part of the basalt sequence at a depth of *c.* 2.7 km which corresponds to average confining pressure of 0.9 kbar.

ACKNOWLEDGEMENTS

We thank the management of Eti Bakır A. Ş. for support in the field. We are grateful to E. Bozkurt, P. A. Floyd and two anonymous referees for their constructive comments on the manuscript. Abidin Temel is acknowledged for whole-rock XRF analyses. We also thank Tijen Üner, Kenan Erol, Dilek Turan, İnan Ulusoy, Ebru and Okan

Delibaş for help with drafting the figures, and Erkan Aydar, Tekin Yürür, Atilla Çiner, David Southarland and İrfan Bayraktar for careful and extensive reviews.

REFERENCES

Arai S. 1984. Pressure-temperature dependent compositional variation of phlogopitic micas in upper mantle peridotites. *Contributions to Mineralogy and Petrology* **87**: 260–264.

Arai S, Natsuko T. 1989. Formation and compositional variation of phlogopites in the Horoman peridotite complex, Hokkaido, northern Japan: implications for origin and fractionation of metasomatic fluids in the upper mantle. *Contributions to Mineralogy and Petrology* **101**: 165–175.

Argyriadis I. 1975. Mésogée permienne, chaîne hercynienne et cassure téthysienne. *Bulletin de la Société Géologique de France* **17**: 56–67.

Aydın M, Şahintürk O, Serdar HS, Özçelik Y, Akarsu İ, Üngör A, Çokraş R, Kasar S. 1986. The geology of the area between Ballıdağ and Çangaldağ (Kastamonu). *Geological Bulletin of Turkey* **29**: 1–16 (in Turkish with English abstract).

Aydın M, Demir O, Özçelik Y, Terzioğlu N, Satır M. 1995. A geological revision of İnebolu, Devrekani, Ağlı and Küre areas: new observations in Paleotethys-Neotethys sedimentary successions. In *Proceedings of the International Symposium on the Geology of the Black Sea Region*, Erler A, Ercan T, Bingöl E, Örçen S (eds). Mineral Research and Exploration Institute of Turkey (MTA) Publications: Ankara; 33–44.

Bailey EH, Barnes JW, Kupfer DH. 1967. Geology and ore deposits of the Küre District, Kastamonu Province, Turkey. In *CENTO Summer Training Program in Geological Mapping Techniques*: 11–94.

Ballhaus C, Berry RF, Green DH. 1991. High pressure experimental calibration of the olivine-orthopyroxene-spinel oxygen geobarometer: implications for the oxidation state of the upper mantle. *Contributions to Mineralogy and Petrology* **107**: 27–40.

Beccaletto L, Jenny C. 2004. Geology and correlation of the Ezine Zone: a rhodope fragment in NW Turkey? *Turkish Journal of Earth Sciences* **13**: 145–176.

Benn K, Laurent R. 1987. Intrusive suite documented in the Troodos ophiolite plutonic complex, Cyprus. *Geology* **15**: 821–824.

Benn K, Nicolas A, Reuber I. 1988. Mantle-crust transition zone and origin of wehrlitic magmas: evidence from the Oman ophiolite. *Tectonophysics* **151**: 75–85.

Boztuğ D, Debon F, Le Fort P, Yılmaz O. 1995. High compositional diversity of the Middle Jurassic Kastamonu plutonic belt, Northern Anatolia, Turkey. *Turkish Journal of Earth Sciences* **4**: 67–86.

Browning P, Smewing JD. 1981. Processes in magma chambers beneath spreading axes: evidences for magmatic associations in the Oman ophiolite. *Journal of the Geological Society, London* **138**: 279–280.

Çakır Ü. 1995. Geological characteristics of the Aşıköy-Toykondu (Küre-Kastamonu) massive sulfide deposits. *Mineral Research and Exploration Institute of Turkey (MTA) Bulletin* **117**: 29–40.

Dick HJB, Bullen T. 1984. Chromian spinel as a petrogenetic indicator in abyssal and alpine-peridotites and spatially associated lavas. *Contributions to Mineralogy and Petrology* **86**: 57–76.

Eren RH. 1979. *The Geological and Petrographical Study of the Metamorphites at Kastamonu-Taşköprü Area*. PhD Thesis, İstanbul Technical University Turkey (in Turkish with English abstract).

Erler A. 1995. Wall rock alteration and trace element content at Aşıköy-Küre massive sulfide deposit (Kastamonu-Turkey. In *Proceedings of the International Symposium on the Geology of the Black Sea Region*, Erler A, Ercan T, Bingöl E, Örçen S (eds). Mineral Research and Exploration Institute of Turkey (MTA) Publications: Ankara; 214–218.

Girardeau J, Mercier JC. 1992. Evidence for plagioclase-lherzolite intrusion in the Mid-Atlantic Ridge, DSDP Leg 37. In *Ophiolites and Their Modern Oceanic Analogues*, Parson L, Murton BJ, Browning P (eds). Special Publication 60. Geological Society: London; 241–250.

Göncüoğlu MC, Kuwahara K, Tekin UK, Turhan N. 2004. Upper Permian (Changxingian) radiolarian cherts within the clastic successions of the ''Karakaya Complex'' in NW Anatolia. *Turkish Journal of Earth Science* **13**: 201–213.

Güner M. 1980. Geology and massive sulfide ore of the Küre Area, the Pontic Ranges, northern Turkey. *Mineral Research and Exploration Institute of Turkey (MTA) Bulletin* **93/94**: 65–109 (in Turkish with English abstract).

Irvine TN. 1967. Chromian spinel as a petrogenetic indicator; part 2, petrologic applications. *Canadian Journal of Earth Sciences* **4**: 71–103.

JICA and MMAJ 1992. *The Republic of Turkey Report on the Mineral Exploration of Küre Area*. Etibank Report: Ankara.

Juteau T, Ernewein M, Reuber I, Whitechurch H, Dahl R. 1988. Duality of magmatism in the plutonic sequence of the Sumail Nappe, Oman. *Tectonophysics* **15**: 107–135.

Karson JA, Elthon DL, Delong SSE. 1983. Ultramafic inclusions in the Lewis Hills Massif, Bay of Islands ophiolite complex, Newfoundland: implications of igneous processes at oceanic fracture zones. *Geological Society of America Bulletin* **94**: 307–320.

Ketin İ. 1962. *Explanatory Text of the Geological Maps of Turkey, Sinop Sheet*. Mineral Research and Exploration Institute of Turkey (MTA) Publications: Ankara.

Ketin İ, Gümüş Ö. 1962. *Geology of the Sinop, Ayancık and Areas to the South of These Towns*. TPAO Report: Ankara (in Turkish).

Kovenko V. 1944. Metallogeny of the old copper body and recently discovered Aşıköy body, and central and eastern part of coastal regions of Black Sea. *MTA Bulletin* **2**: 180–211 (in Turkish with English abstract).

Kozur HW, Aydın M, Demir O, Yakar H, Göncüoğlu MC, Kuru F. 2000. New stratigraphic and palaeogeographic results from the Palaezoic and Early Mesozoic of the Middle Pontides (Northern Turkey) in the Azdavay, Devrekani, Küre and İnebolu Areas: implications for the Carboniferous–Early Cretaceous geodynamic evolution and some related remarks to Karakaya Oceanic Rift Basin. *Geologia Croatia* **53**: 209–268.

Kutluk H, Bozdoğan N. 1981. *Preliminary Report of Palynology in the Sediments of Late Palaeozoic–Lower Mesozoic of the Region IV*. TPAO Report: Ankara (in Turkish).

Laurent R. 1992. Peridotite intrusions emplaced in the fossil suprasubduction zone environment of Cyprus. In *Ophiolites and Their Modern Oceanic Analogues*, Parson L, Murton BJ, Browning P (eds). Special Publication 60. Geological Society: London; 233–239.

Leake BE, Woolley AR, Arps CES, Birch WD, Gilbert MC, Grice JD, Hawthorne FC, Kato A, Kisch HJ, Krivovichev VG, Linthout K, Laird J, Mandarino J, Maresh WV, Nickel EH, Rock NMS, Schumacher JC, Smith DC, Stephenson NCN, Ungaretti L, Whittaker EJW, Youzhi G. 1997. Nomenclature of amphiboles: report of the Subcommittee on Amphiboles of the International Mineralogical Association, Commission on New Minerals and Mineral Names. *The Canadian Mineralogist* **35**: 219–246.

Lindsley DH. 1983. Pyroxene thermometry. *American Mineralogist* **68**: 477–493.

Lippard SJ, Shelton AW, Gass IG. 1986. *The Ophiolite of Northern Oman*. Geological Society of London Memoir 11.

Mattioli GS, Baker MB, Rutter MJ, Stolper EM. 1989. Upper mantle oxygen fugacity and its relationship to metasomatism. *Journal of Geology* **97**: 521–536.

Mitchell AH, Bell JD. 1973. Island-arc evolution and related mineral deposits. *Journal of Geology* **81**: 381–405.

Molin G, Zanazzi PF. 1991. Intracrystalline Fe^{2+}-Mg ordering in augite: experimental study and geothermometric applications. *European Journal of Mineralogy* **3**: 863–875.

Nimis P. 1995. A clinopyroxene geobarometer for basaltic systems based on crystal-structure modeling. *Contributions to Mineralogy and Petrology* **121**: 115–125.

Okay Aİ, Altıner D. 2004. Uppermost Triassic limestones in the Karakaya Complex—stratigrafic and tectonic significance. *Turkish Journal of Earth Sciences* **13**: 187–199.

Okay Aİ, Göncüoğlu MC. 2004. The Karakaya Complex: a review of data and concepts. *Turkish Journal of Earth Sciences* **13**: 77–95.

Okay Aİ, Tüysüz O, Satır M, Altiner SÖ, Altıner D, Sherlcok S, Eren R. 2005. The structure and geological evolution of the Central Pontides. *58th Geological Congress of Turkey, Ankara, Abstracts*: 315–336.

Önder F, Boztuğ D, Yılmaz O. 1987. New paleontological data (Conodont) from the Lower Mesozoic rocks of the Göynükdağı-Kastamonu region at the Western Pontides, Turkey. *Melih Tokay Geology Symposium, Ankara, Abstracts*: 127–128 (in Turkish).

Pehlivanoğlu H. 1985. *Geology of the Küre-Kastamonu Pyritic Copper Deposits (Bakibaba-Aşıköy) and the Surrounding Rocks*. MTA Report 1744 (in Turkish).

Pickett EA, Robertson AHF. 2004. Significance of the Triassic volcanogenic Nilüfer Unit for Paleotethys and Karakaya suture zone in NW Turkey. *Turkish Journal of Earth Sciences* **13**: 97–143.

Roeder PL, Campbell IH. 1985. The effect of postcumulus reactions on composition chrome-spinels from Jimberlana intrusion. *Journal of Petrology* **26**: 763–786.

Simkin T, Smith JU. 1970. Minor element distribution in olivine. *Journal of Geology* **78**: 304–325.

Şengör AMC, Yılmaz Y, Ketin İ. 1980. Remnants of pre-Late Jurassic ocean in northern Turkey: fragments of Permian-Triassic Paleo-Tethys? *Geological Society of America Bulletin* **91**: 599–609.

Smewing JD. 1980. Regional setting and petrological characteristics of the Oman ophiolite in northern Oman. *Ofioliti* **2**: 335–378.

Terzioğlu N, Satır M, Saka K. 2000. Geochemistry and geochronology of basaltic rocks of the Küre Basin, Central Pontides (N-Turkey). In *Proceedings of the International Earth Sciences Colloquium of the Aegean Region, İzmir*: 219.

Turhan N, Okuyucu C, Göncüoğlu MC. 2004. Autochthonous Upper Permian (Midian) carbonates in the Western Sakarya Composite Terrane, Geyve Area, Turkey: preliminary data. *Turkish Journal of Earth Sciences* **13**: 215–229.

Ustaömer T, Robertson AHF. 1993. Late Palaeozoic–Early Mesozoic marginal basins along the active southern continental margin of Eurasia: evidence from the Central Pontides (Turkey) and adjacent regions. *Geological Journal* **28**: 219–238.

Ustaömer T, Robertson AHF. 1994. Late Palaeozoic marginal basin and subduction-accretion: evidence from the Palaeotethyan Küre Complex, Central Pontides, northern Turkey. *Journal of Geological Society, London* **151**: 291–306.

Ustaömer T, Robertson AHF. 1995. Palaeotethyan tectonic evolution of the North Tethyan Margin in the Central Pontides, N. Turkey. In *Proceedings of the International Symposium on the Geology of the Black Sea Region*, Erler A, Ercan T, Bingöl E, Örçen S (eds). Mineral Research and Exploration Institute of Turkey (MTA): Ankara; 24–32.

Ustaömer T, Robertson AHF. 1997. Tectonic-sedimentary evolution of the north Tethyan margin in the central Pontides of northern Turkey. In *Regional and Petroleum Geology of the Black Sea and Surrounding Region*, Robinson AG (ed.). Memoir 68. American Association of Petroleum Geologists 255–290.

Ustaömer T, Robertson AHF. 1999. Geochemical evidence used to test alternative plate tectonic models for pre-Upper Jurassic (Palaeotethyan) units in the Central Pontides, N Turkey. *Geological Journal* **34**: 25–53.

Wınkler HGF. 1975. *Petrogenesis of Metamorphic Rocks* (fourth edition). Springer-Verlag: New York.

Yılmaz O. 1980. Lithostratigraphic units and tectonics of Northeastern part of the Daday-Devrekani Massif (Western Pontides, Turkey). *Publication of Institute of Earth Sciences of Hacettepe University* **5–6**: 101–135 (in Turkish with English abstract).

Yılmaz O, Boztuğ D. 1986. Kastamonu granitoid belt of northern Turkey: first arc plutonism product related to the subduction of the Paleo-Tethys. *Geology* **4**: 179–183.

Yılmaz Y, Şengör AMC. 1985. Palaeo-Tethyan ophiolites in northern Turkey: petrology and tectonic setting. *Ofioliti* **10**: 485–504.

Scientific editing by Erdin Bozkurt

